Available online at www.sciencedirect.com
SCIENCE DIRECT®
Journal of Sound and Vibration 283 (2005) 957–969
JOURNAL OF SOUND AND VIBRATION
www.elsevier.com/locate/jsvi

Some considerations on the effects of the **P**-derivatives on bridge deck flutter

Xin Zhang[a,*], James Mark William Brownjohn[b]

[a]*School of CEE, Nanyang Technological University, 50 Nanyang Avenue, Singapore 639798, Singapore*
[b]*School of Engineering, University of Plymouth, Drake Circus, Plymouth PL4 8AA, UK*

Received 16 June 2003; received in revised form 18 May 2004; accepted 25 May 2004
Available online 11 November 2004

Abstract

Using two degrees of freedom (dof) experimental flutter derivatives to perform three-dimensional flutter analysis for a cable-supported bridge is a widely practiced method. It is important to consider the **P**-derivatives effect to have more accurate analysis for a long-span bridge. Through a case example, this paper studied some of the issues relating to the **P**-derivatives effects on flutter. The operational condition in two-dof experiments was discussed. It was suggested that due to the strong aeroelastic coupling effect of the sectional model studied in this research, there was an inherent weakness of two-dof experiments. The effect of the **P**-derivatives was studied for an example bridge by comparing the flutter analysis results using two-dof and three-dof experimental flutter derivatives.

1. Introduction

Techniques predicting the flutter boundary of cable-supported bridges developed either in frequency domain [1,2], or in time domain [3] are to solve negative damping driven flutter problems.

The structural system by means of its deflection and time derivatives taps off energy from the wind flow. If the system is given an initial disturbance, its motion will either decay or diverge

*Corresponding author.
E-mail addresses: cxzhang@ntu.edu.sg (X. Zhang), james.brownjohn@plymouth.ac.uk (J.M.W. Brownjohn).

0022-460X/$ - see front matter © 2004 Elsevier Ltd. All rights reserved.
doi:10.1016/j.jsv.2004.05.031

Nomenclature

$A_i^*, (i = 1, ..., 6)$	flutter derivatives
$A_{ij}(K)$	variables in E_{ij}
B	width of the bridge deck
$B_{ij}(K)$	variables in E_{ij}
dm	infinite small mass
E	impedance matrix
E_{ij}	element in impedance matrix
$G_{r_i s_j}$	modal integral
h_i	ith vertical mode
$H_i^*, (i = 1, ..., 6)$	flutter derivatives
I_i	generalized inertia
K	reduced frequency
l	bridge deck length
p_i	ith lateral mode
$P_i^*, (i = 1, ..., 6)$	flutter derivatives
U, V, S	matrices
α_i	ith rotational mode
ω_i	circular frequency
$\bar{\xi}$	participation factor vector of structural modes at flutter
η_i	the ith full bridge mode shape

according to whether the energy of motion extracted from the flow is less than or exceeds the energy dissipated by the system through mechanical damping. The dividing line between the decay and divergent case, namely, sustained sinusoidal oscillation, is recognized as the critical flutter condition, the threshold of negative damping.

The energy flow between the structure and the surrounding flow is characterized by two sets of parameters: flutter derivatives [4] and structural mode shapes. The flutter derivatives are measured via experiments with rigid sectional models, which do not show instability within the reduced velocity range covered by the experiments. By incorporating the effect of mode shapes of a flexible structure, these flutter derivatives may change some particular aeroelastic modal damping of the interactive system from positive to negative. At the critical wind speed, it is reasonable to postulate that a single aeroelastic mode will approximate the total response. This assumption is justifiable from observation of the fact that typically just one predominant mode will become unstable and dominate the flutter response of a three-dimensional bridge model in the wind tunnel. It has been common to use the combination of a set of mechanical modes, namely the modes of the bridge deck under non-wind condition, as the flutter mode to perform the flutter analysis.

While the flutter mode is described in three dimensions, the flutter derivatives are usually identified experimentally from a two-dimensional sectional model, which represents a strip of the full bridge deck. Totally 18 flutter derivatives describe the aeroelastic property of a sectional model with three degrees of freedoms (dofs). Due to the difficulties in the identification of these 18 parameters, two-dof results are usually obtained in the experiments. The use of two-dof flutter derivatives in three-dimensional flutter analysis is supported by the assumption that the **P**-related derivatives have a stabilizing effect on flutter. If they were omitted, the analytical result would be conservative.

In the two-dof experiments, however, confinement must be applied to the sectional model to prevent the model from oscillating in the lateral direction. If the sectional model experiences aeroelastic coupling, the confinement in the lateral direction may affect the model motion in other directions through the aeroelastic coupling effect. In this case, the two-dimensional experimental result could be affected.

Previous researches pertaining to the identification of two- and three-dof flutter derivatives performed by Singh et al. [5], Chen et al. [6] and others mainly concentrate on the identification algorithm. The flutter derivatives are considered as constitutive quantities, independent of measurement methods. This is true when the experimental condition is controlled ideally. Under the operational condition, however, the two-dof identification result may be affected by external factors, such as the physical lateral restraint.

Furthermore, the lateral confinement on the sectional model is equivalent to applying additional restraints on the prototype. These restraints confine the structure in the aeroelastic sense rather than allowing it to vibrate freely without causing any aeroelastic forces in the lateral direction. For a structure that is more confined, a higher flutter wind speed is usually expected. This might not give rise to a conservative design. A previous study by Katsuchi et al. [7] on Akashi-Kaikyo Bridge suggests that the lateral derivatives have a significant effect on the flutter wind speed. When **P**-derivatives are considered, in their particular case, there is a notable decrement of the flutter wind speed.

In order to discuss these issues, it is needed to distinguish the following three cases where

(A) the sectional model is tested in two-dof experiments with the third degree of freedom confined;
(B) the sectional model is tested in three-dof experiments for 18 flutter derivatives among which P-related flutter derivatives are assigned zero and
(C) the sectional model is tested in three-dof experiments for 18 flutter derivatives all of which are used in the flutter analysis.

Based on the classification above, it should be Case B instead of Case A that reflects the assumption of omitting the **P**-related derivatives in the flutter analysis of a full bridge. These three cases are studied in this research for one particular bridge section type.

2. Experimental flutter derivatives

A partially streamlined box girder sectional model with extended wings on each side (Fig. 1) was tested [8]. The suspension and measurement system is shown in Fig. 2. The system identification method used is eigensystem realization algorithm (ERA) [9]. The identified flutter derivatives of two- and three-dof are shown in Fig. 3a–c.

In Fig. 3c, the aeroelastic coupling between the lateral and the rotational dof is indicated by large value of P_3^*. Due to the aeroelastic coupling effect, the orthogonality of the modal coordinate for the sectional model is affected. Under this situation, the restraints in the lateral direction, which are considered orthogonal to the rotational dof under no wind condition, now can be felt by the rotation motion. The behavior of the rotational vibration is expected to be affected by the lateral restraining force. Therefore, the two-dof experiment may not produce accurate results. This could be part of the reason for the differences in the flutter derivative ($H_1^* \sim H_4^*$, $A_1^* \sim A_4^*$) between two- and three-dof experiments.

It should be mentioned that the differences might also result from the inaccuracy of the identification.

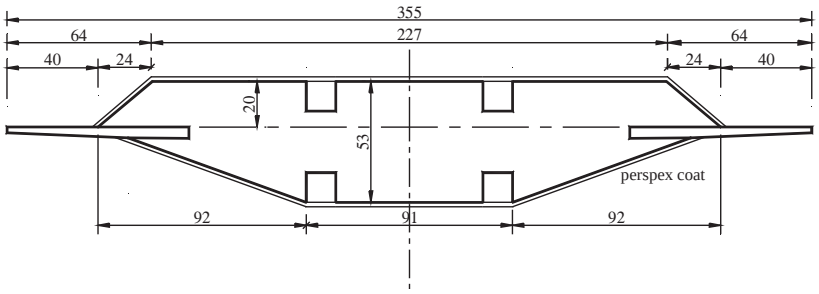

Fig. 1. Streamlined box girder model (dimension mm).

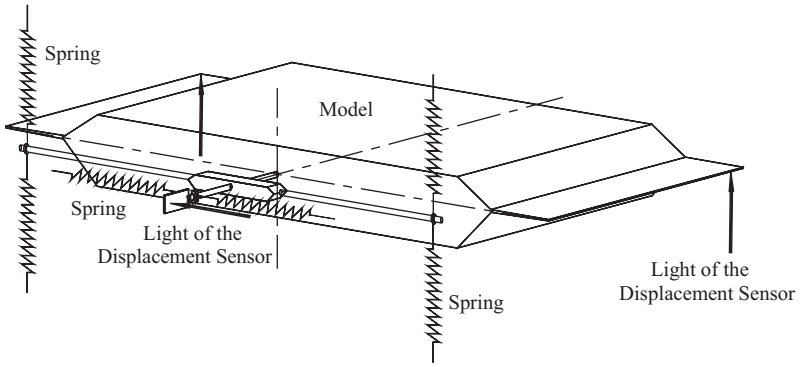

Fig. 2. Setup for free vibration test (one end).

It seems that the other coupling term between rotational and lateral dof, A_6^*, will not affect the two-dof experiments as much as P_3^* does because, in the two-dof experiment, the lateral motion is very weak and thus can only generate a small coupling force through A_6^* to affect the rotational motion.

The same discussion applies to P_6^* and H_6^* for the aeroelastic coupling in vertical and lateral dof.

In this case example, the existence of the aeroelastic coupling between the lateral and the other two dofs suggests that all the three dofs are coupled together inherently in wind. Constraints on the lateral dof may block the energy flow among the three dofs. An analysis which omits the **P**-derivatives might not be accurate. To evaluate the **P**-derivatives effect on flutter, it is needed to distinguish between the three different cases mentioned in the section of introduction. A study on a full bridge is performed in the following part.

3. The suspension bridge and aeroelastic modeling

The main span of the example bridge is 1410 m, with side spans of 530 and 280 m. The steel box sections are 22 m wide and 4.5 m deep and the shape is the same as the box girder sectional model. The towers are box section, 6×6 m at the base and 4.5×4.5 at the tower tops.

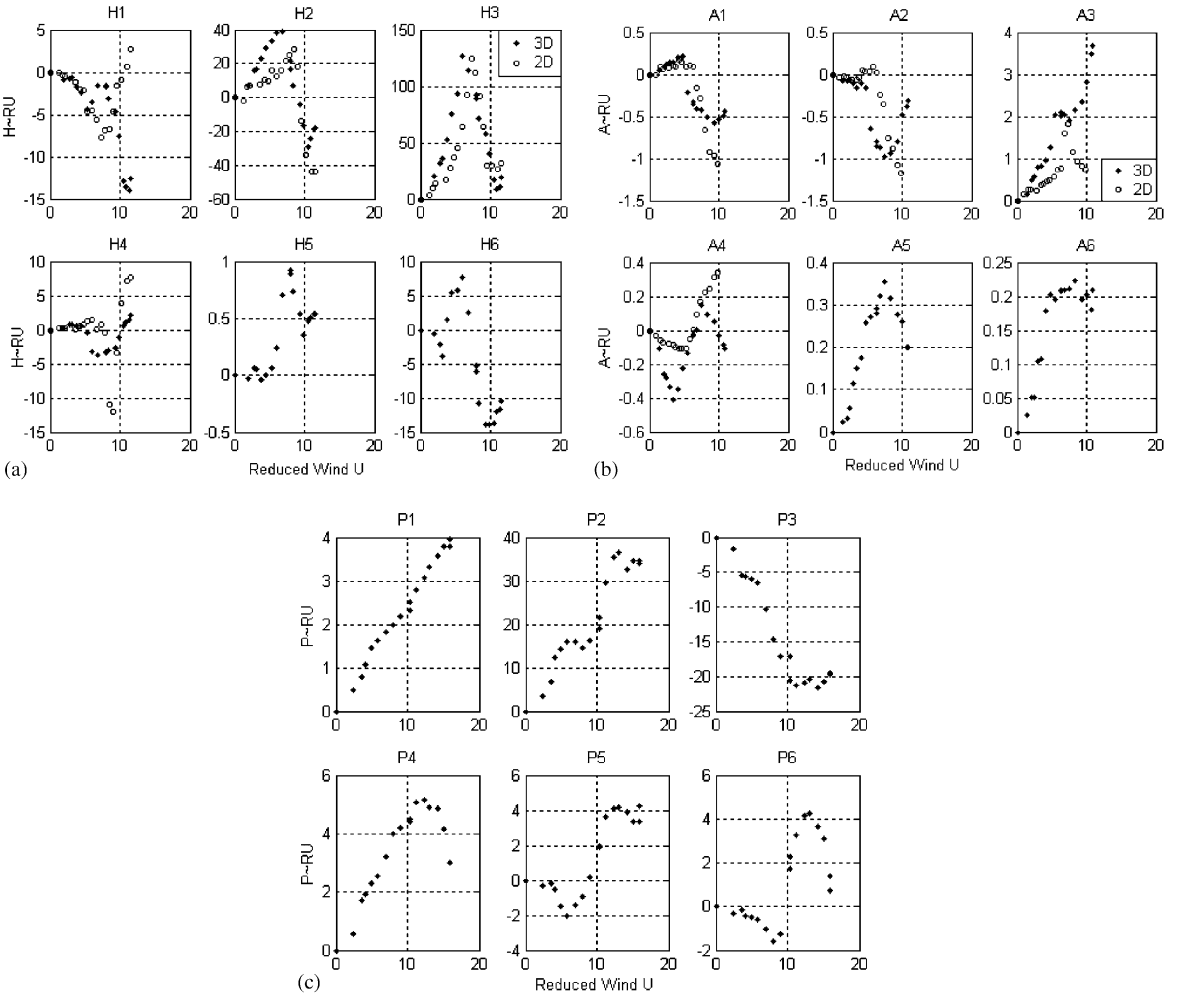

Fig. 3. Flutter derivatives: (a) $(H_i^*, i = 1, \ldots, 6)$, (b) $(A_i^*, i = 1, \ldots, 6)$, and (c) $(P_i^*, i = 1, \ldots, 6)$.

To facilitate the inclusion of an aeroelastic load, 3-D beam deck formulation was used to model the deck structure. Spar elements (no flexural stiffness) were used to represent the main cable and hanger. They have the facility to accommodate the initial strain value. The tower was analyzed using beam elements with tension, compression, torsion and bending capabilities.

Modal analysis was first conducted. The resultant first 10 deck modes are listed in Table 1. After these modal parameters were obtained, they were used for the flutter instability prediction. The frequency domain flutter prediction method developed by Jain et al. [2] was used. The nature of this method is to solve an aeroelastically influenced eigen-problem:

$$|E| = 0. \tag{1}$$

Table 1
Dynamic properties of the bridge

Mode no.	Mode type	Frequency n_i (Hz)
1	L, 1st S	0.0688
2	1st V, S	0.1277
3	L, 1st AS	0.1591
4	V 1st AS	0.1646
5	V 2nd S	0.1897
13	V 2nd AS	0.2498
14	L 2nd S; T 1st S	0.2816
16	V 3rd S	0.3246
26	V 3rd AS	0.4022
28	T 1st AS	0.45853

Note: S = symmetrical; AS = anti-symmetrical; V = vertical; LT = lateral-torsion; and T = torsion.

The general term of the impedance matrix E is

$$E_{ij} = -K^2\delta_{ij} + \mathrm{i}KA_{ij}(K) + B_{ij}(K), \tag{2}$$

where $\mathrm{i} = \sqrt{-1}$,

$$A_{ij}(k) = 2\zeta_i K_i \delta_{ij} - \frac{\rho B^4 lK}{2I_i}[H_1^* G_{h_i h_j} + H_2^* G_{h_i \alpha_j} + H_5^* G_{h_i p_j} + P_1^* G_{p_i p_j} + P_2^* G_{p_i \alpha_j} + P_5^* G_{p_i h_j} + A_1^* G_{\alpha_i h_j} + A_2^* G_{\alpha_i \alpha_j} + A_5^* G_{\alpha_i p_j}] \tag{3}$$

and

$$B_{ij}(k) = K_i^2\delta_{ij} - \frac{\rho B^4 lK^2}{2I_i}[H_3^* G_{h_i \alpha_j} + H_4^* G_{h_i h_j} + H_6^* G_{h_i p_j} + P_3^* G_{p_i \alpha_j} + P_4^* G_{p_i p_j} + P_6^* G_{p_i h_j} + A_3^* G_{\alpha_i \alpha_j} + A_4^* G_{\alpha_i h_j} + A_6^* G_{\alpha_i p_j}]. \tag{4}$$

In Eqs. (2)–(4), ρ is air density, B is the deck width, l is the deck length, $K = B\omega/U$ is the reduced frequency, $K_i = B\omega_i/U$ is the reduced frequency of mode i, H_m^*, A_m^*, P_m^*, $(m = 1, \ldots, 6)$ are flutter derivatives and δ_{ij} is the Kronecker delta function defined as

$$\delta_{ij} = \begin{cases} 1, & i = j, \\ 0, & i \neq j, \end{cases} \tag{5}$$

The modal integrals $G_{r_i s_j}$ are obtained by integration over the length of the deck, which is the primarily aerodynamic load source

$$G_{r_i s_j} = \int_0^l r_i(x)\, s_j(x) \frac{\mathrm{d}x}{l}, \tag{6}$$

where $r_i = h_i, p_i$ or α_i and $s_j = h_j, p_j$ or α_j are the ith and jth mode shapes in the vertical, lateral and rotational direction, respectively.

4. The flutter analysis result

The analysis is carried out in three steps. In the first step, the analysis is performed with two-dof flutter derivatives (Case A), and the critical wind speeds for flutter are obtained. In the second step, two-dof flutter derivatives are obtained from three-dof flutter derivatives by setting the **P**-related derivatives to zero for all the reduced velocity range, i.e., $P_1^* \sim P_6^* = 0$; $A_5^* = A_6^* = 0$; $H_5^* = H_6^* = 0$ (Case B). In the third step, analysis is carried out with three-dof flutter derivatives (Case C). The first step indicates that the self-excited load in the lateral direction is constrained; the second step assumes that there is a self-excited load relating to lateral vibration but it is neglected; and the third step fully considers self-excited forced in three dofs.

Eq. (1) is doubled since both the real and imaginary parts of the determinant have to be zero. Corresponding unknowns are reduced frequency K or wind velocity U and vibration frequency ω. These equations are highly nonlinear in both unknowns not only through the dependence that appears in the expression of the elements in impedance matrix, but also through the flutter derivatives that are implicit in these expressions. A graphical method was proposed by Astiz [10]. In this method, it is necessary to first compute $|E|$ for an array of $K \sim \omega$ values: this is equivalent to defining two surfaces, one for the real part and the other for the imaginary part of $|E|$. The intersection of these two surfaces with $K \sim \omega$ plane is obtained by linear interpolation. Then the zero contour curves of the real surface and imaginary surface are obtained with piecewise linear approximation and their intersections can be determined either numerically or graphically. The intersection points define the flutter condition.

Figs. 4a–c show the plot of contour lines for impedance matrix of zero determinant value from the three study cases mentioned above. The intersection points of the solid line (zero value contour line of real part of the determinant of the impedance matrix) and the dash line (zero value contour line of imaginary part) define the flutter condition. Table 2 summarizes the analysis cases and the corresponding flutter wind speeds and frequencies.

It can be observed that there are two flutter conditions found in the analysis of Case A and B, but only one flutter condition found for Case C. The lowest wind speed for flutter occurs in Case B, i.e. the case which uses the three-dof flutter derivatives with all **P**-related flutter derivatives being assigned zero. The lowest flutter wind velocity in this case is 38.5 m/s. The flutter frequency is 0.252 Hz. Two-dof flutter derivatives give rise to the highest flutter wind speed: 53 m/s and flutter frequency 0.267 Hz. Case C produces the flutter wind velocity 48m/s and flutter frequency 0.332 Hz.

The observation in Figs. 4a–c suggests that the flutter frequency in Case C is very close to the second flutter frequency in Case B. This might suggest that the fundamental flutter mode in Case C corresponds to the second flutter mode in Case B. If this is true, omitting the **P**-related derivatives may change the shape of the fundamental flutter mode. This phenomenon is quite reasonable because in Eqs. (3) and (4), flutter derivatives are coupled with the modal integrals. Any changes in the flutter derivatives will be equivalent to changes in the participation of the

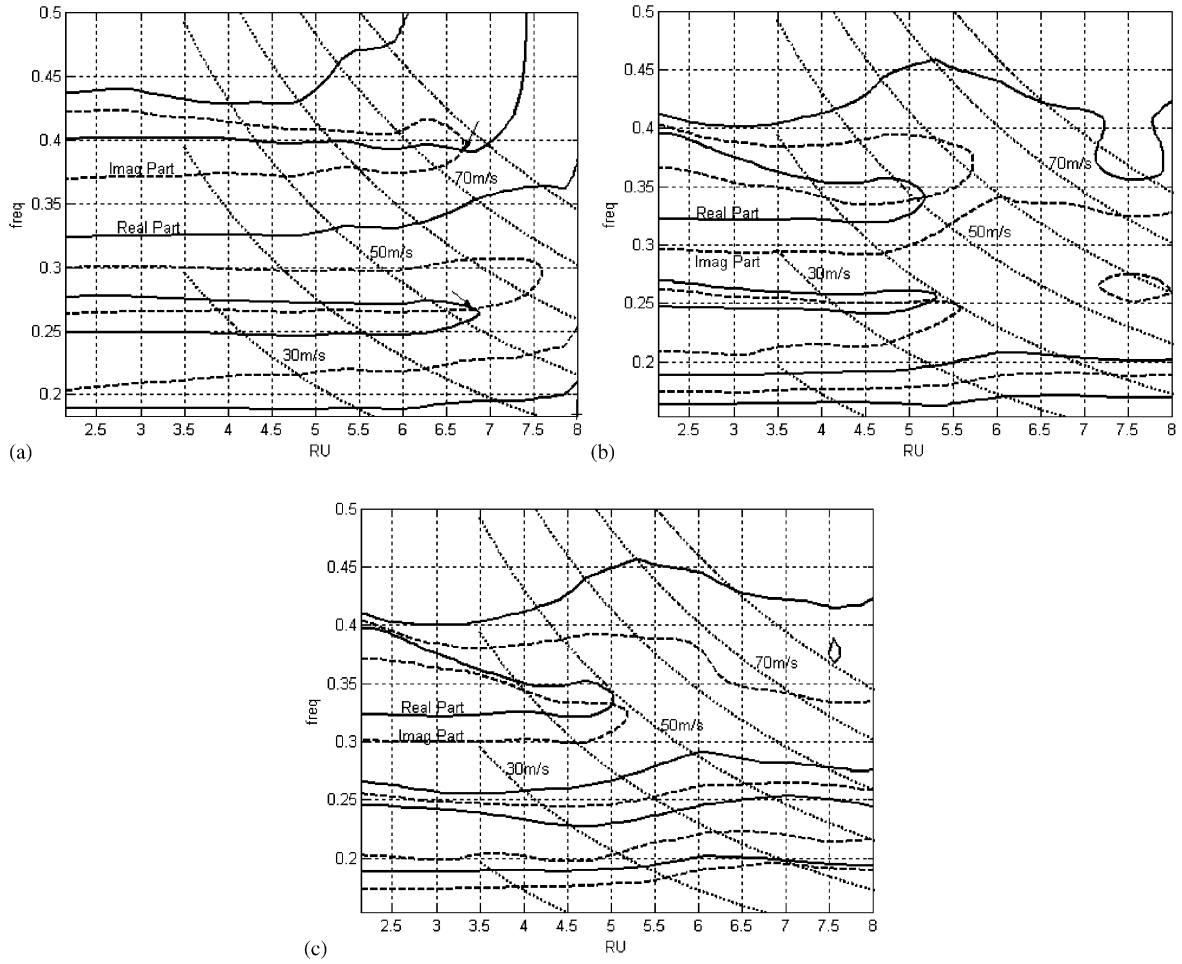

Fig. 4. E Matrix in (a) Case A, (b) Case B, and (c) Case C.

Table 2
Flutter speeds and frequencies

Case	Deck mode combination	Flutter speed, U_{flutter} (m/s)	Flutter frequency, f_{flutter} (Hz)	
52.7		75.9	0.267	0.392
38.5	1, 2, 3, 4, 5, 13, 14, 16, 26, 28	51.1	0.252	0.341
Case C		48.2	NA	0.332	NA

NA: Solution not found within the reduced velocity range covered by experiment.

modal integrals and finally equivalent to changes in the analytical modal flutter result. This statement, however, needs to be verified by solving not only the analytical flutter frequencies but also flutter mode shapes.

The solution of

$$E_{\text{flutter}}\bar{\xi} = 0 \tag{7}$$

at flutter determines the participation magnitude of each mechanical mode. Because the flutter frequency is solved numerically, the determinant of impedance matrix obtained at flutter is not strictly zero, i.e.

$$|E|_{\text{flutter}} \approx 0. \tag{8}$$

Solving Eq. (7) directly will not always give a reasonable result. Some care should be exercised to solve the equation, due to the numerical sensitivity of the system at flutter. It was argued [11] that typically for suspension bridges, a single torsional mode is the most likely mode to dominate flutter while the participation of other modes may not significantly alter the outcome of the analysis. Therefore, for practical reasons, the preset value should be assigned to the entry corresponding to such flutter dominating modes. Otherwise, misleading results may be obtained.

However, some analytical results of multimode flutter analysis of long-span bridges indicate that because of the closely spaced natural frequencies and three-dimensional mode shapes, the aerodynamic coupling mechanism among modes becomes complex. The flutter is not always initiated by the fundamental symmetric torsional mode [12,13]. These results seem to be sensitive to the structural and aerodynamic characteristics of the system.

A systematic method to solve the flutter mode is equivalent to finding an exact singular matrix $\tilde{E}$, so that the numerically obtained impedance matrix can be approximated with its main structure maintained and the solution of equation $\tilde{E}\bar{\xi} = 0$ producing approximately the real eigenvector.

In this study, the solution is obtained by singular value decomposition (SVD) of the impedance matrix, i.e. $E = USV^{\mathrm{T}}$, where U and V are orthogonal singular vectors matrices and S is the diagonal singular value matrix. By assigning the last singular value to zero, Eq. (7) is approximated and solved as follows:

$$U^{\mathrm{T}}E\bar{\xi} \approx \begin{bmatrix} S_1 & 0 \\ 0 & 0 \end{bmatrix} V^{\mathrm{T}}\bar{\xi} = 0. \tag{9}$$

Figs. 5–7 show the calculated flutter mode shape. All the figures indicate that the vertical motion predominates in the flutter mode. It can be seen that the fundamental flutter mode shape corresponding to Case C is similar to the second flutter mode in the other two cases.

The **P**-derivatives push the lower one of the two unstable modes to higher reduced wind velocity, which is outside the experimental range. It seems the energy in the vertical and rotational modes flows into the lateral mode and is dissipated by the **P**-derivatives in Case C. In Case B, however, by setting the **P**-related derivatives to zero, the modal integrals in the impedance matrix containing lateral mode component are deactivated. The energy exchanging process is stopped. The energy stays inside the system resulting in instability of the system.

On the other hand, the higher frequency flutter mode, which occurs in all three case studies, seems to show a different behavior. For this flutter mode, the **P**-derivatives must be contributing

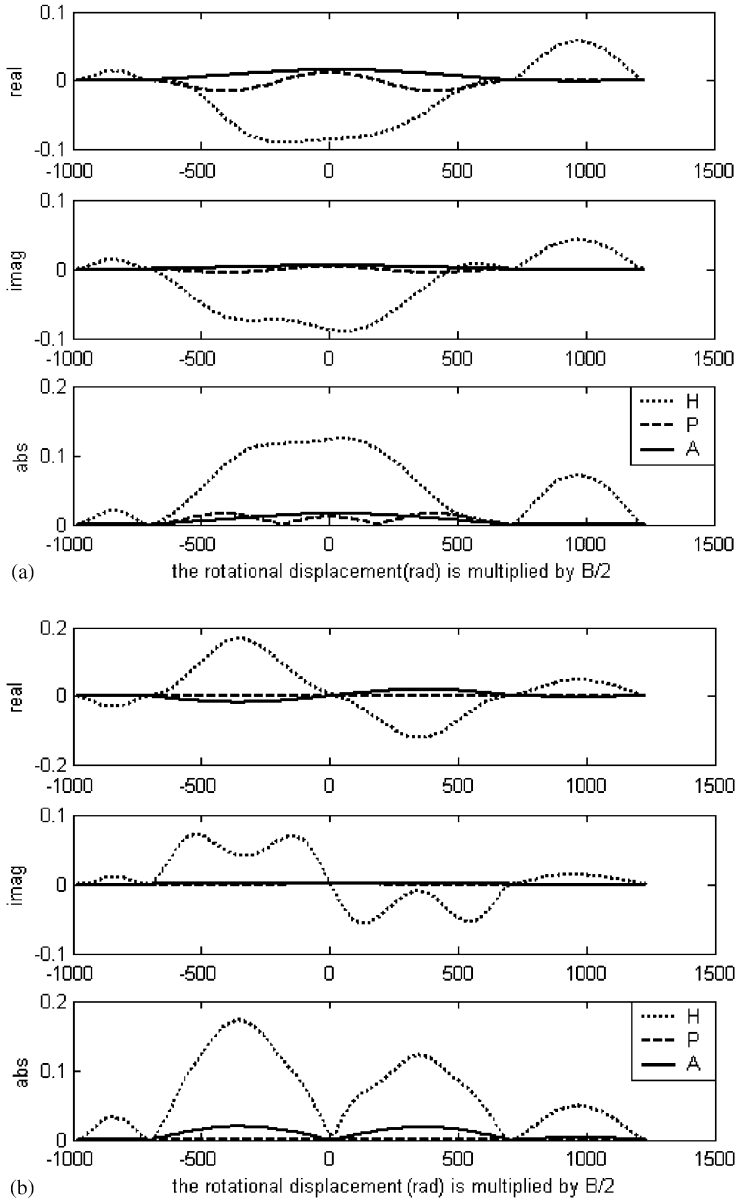

Fig. 5. (a) First flutter mode in Case A, and (b) second flutter mode in Case A.

energy to the response via the modal integrals resulting in a lower flutter wind speed in Case C than in Case B.

The mechanism for flutter derivatives to affect the full bridge flutter boundary seems complex. All the discussions above should be considered as a specific case study of a more general problem.

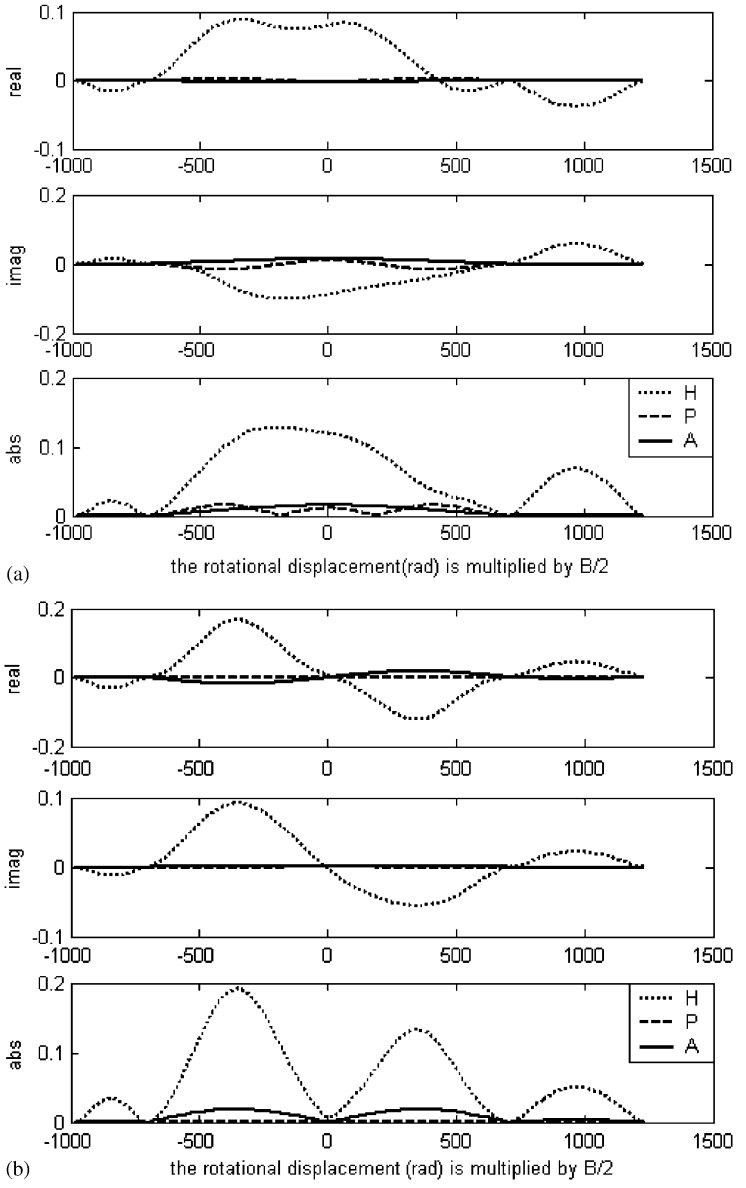

Fig. 6. (a) First flutter mode in Case B, and (b) second flutter mode in Case B.

5. Conclusion

In comparison with two-dof flutter derivative case (Case A) and three-dof flutter derivative case (Case C), the analysis in Case B, where three-dof flutter derivatives with **P**-related flutter derivatives being set to zero gives rise to the lowest flutter wind speed. This might confirm the

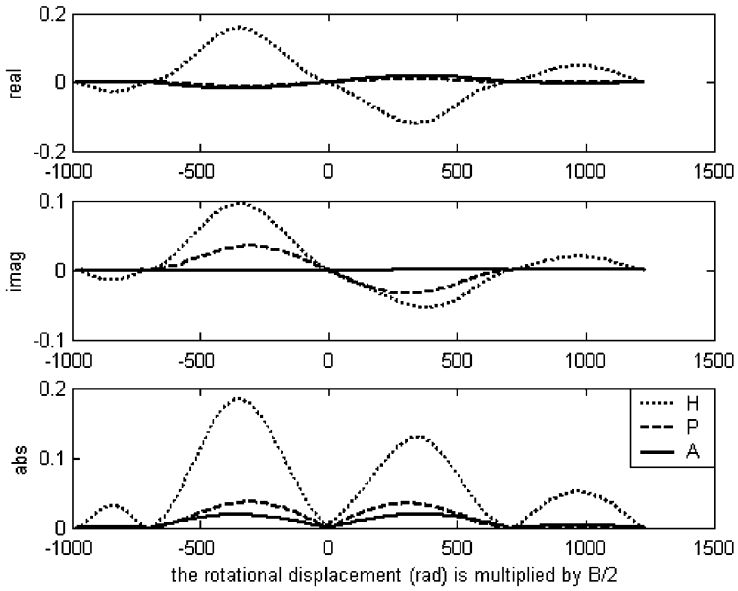

Fig. 7. First flutter mode in Case C.

assumption that the **P**-related flutter derivatives have a stabilizing effect on flutter. The two-dof flutter derivatives produce the highest wind speed for instability, indicating that the current practice of using two-dof experimental results is not necessarily conservative.

In the absence of **P**-derivatives, not only the predicted flutter wind speeds but also the flutter frequencies and mode shapes may be different from what are predicted by using the full set of 18 aeroelastic parameters, indicating the complexity of the mechanism for the aeroelastic parameters to affect the flutter of a full bridge. Conclusions apply to the specific case example in this study.

Reference

[1] R.H. Scanlan, The action of flexible bridges under wind. Part I: Flutter theory, *Journal of Sound and Vibration* 60 (2) (1978) 187–199.

[2] A. Jain, N.P. Jones, R.H. Scanlan, Coupled flutter and buffeting analysis of long-span bridges, *Journal of Structural Engineering* 122 (7) (1996) 716–725.

[3] X. Chen, M. Matsumoto, A. Kareem, Time domain flutter and buffeting response analysis of bridges, *Journal of Engineering Mechanics* 126 (1) (2000) 7–16.

[4] R.H. Scanlan, J.J. Tomko, Airfoil and bridge deck flutter derivatives, *Journal of Engineering Mechanics* 97 (6) (1971) 1717–1737.

[5] L. Singh, N.P. Jones, R.H. Scanlan, O. Lorendeaux, Simultaneous identification of 3-dof aeroelastic parameters, *Proceedings of the Ninth International Conference on Wind Engineering*, Wiley Eastern, New Delhi, India, 1995, pp. 972–981.

[6] A. Chen, X. He, H. Xiang, Identification of 18 flutter derivatives of bridge decks, *Journal of Wind Engineering and Industrial Aerodynamics* 90 (2002) 2007–2022.

[7] H. Katsuchi, N.P. Jones, R.H. Scanlan, Multi-mode coupled flutter and buffeting analysis of the Akashi-Kaikyo Bridge, *Journal of Structural Engineering* 125 (1999) 60–70.

[8] X. Zhang, Aeroelastic Analysis of Super Long Cable-supported Bridges, PhD Thesis, Nanyang Technological University, Singapore, 2003.
[9] J.N. Juang, An eigensystem realization algorithm for modal parameter identification and modal reduction, *Journal of Guidance* 8 (5) (1984) 620–627.
[10] M.A. Astiz, Flutter stability of very long suspension bridges, *Journal of Bridge Engineering* 3 (3) (1998) 132–139.
[11] A. Jain, Multi-mode Aeroelastic and Aerodynamic Analysis of Long-span Bridges, PhD Thesis, Johns Hopkins University, Baltimore, USA, 1997.
[12] T.T.A. Agar, The analysis of aerodynamic flutter of suspension bridges, *Computers and Structures* 30 (1988) 593–600.
[13] T. Miyata, H. Yamada, Coupled flutter estimate of a suspension bridge, *Journal of Wind Engineering and Industrial Aerodynamics* 37 (1988) 485–492.